Physics of Plasmas

RESEARCH ARTICLE | APRIL 01 2024

Ion dynamics in standing electromagnetic wave near the cyclotron resonance

A. Fruchtman ; G. Makrinich

Check for updates

Phys. Plasmas 31, 043502 (2024)
https://doi.org/10.1063/5.0179340

View Online
Export Citation

01 April 2024 17:23:20

AIP Publishing

Ion dynamics in standing electromagnetic wave near the cyclotron resonance

Cite as: Phys. Plasmas **31**, 043502 (2024); doi: 10.1063/5.0179340
Submitted: 1 October 2023 · Accepted: 11 March 2024 ·
Published Online: 1 April 2024

View Online Export Citation CrossMark

A. Fruchtman[a] and G. Makrinich

AFFILIATIONS

H.I.T.-Holon Institute of Technology, 52 Golomb St., Holon 58102, Israel

[a]Author to whom correspondence should be addressed: fnfrucht@hit.ac.il

ABSTRACT

The dynamics of ions under the forces exerted by a planar standing electromagnetic wave near the cyclotron resonance is studied. It is shown that ions whose cyclotron frequency is larger than the wave frequency are pushed by the ponderomotive force toward and oscillate around the wave magnetic node, while ions whose cyclotron frequency is smaller than the wave frequency are pushed to and oscillate around the wave electric node. When the difference between the cyclotron frequency and the wave frequency is large, the ion motion is governed by a time independent ponderomotive potential. When that difference is small, the ion oscillates around the wave magnetic node with varying-in-time amplitude and frequency, described approximately by solutions of the Mathieu equation. Difficulties in using such a configuration for mass separation are discussed.

© 2024 Author(s). All article content, except where otherwise noted, is licensed under a Creative Commons Attribution-NonCommercial 4.0 International (CC BY-NC) license (https://creativecommons.org/licenses/by-nc/4.0/). https://doi.org/10.1063/5.0179340

01 April 2024 17:23:20

I. INTRODUCTION

Mass separation, separation of particles of different mass, is a crucial process in a variety of societal applications.[1–32] In a significant number of techniques, electromagnetic forces are exerted on charged particles or plasmas. These techniques rely on the difference in particle dynamics under electromagnetic forces that result from mass difference. Recently, a tutorial reviewed comprehensively the various mechanisms for plasma mass separation.[1] In early studies, the mass-dependence of the gyro-orbit in a magnetic field was used in mass spectrometry[2] and in the development of the Calutron in the Manhattan project.[3] Later, the mass-dependent centrifugal force in rotating plasmas was used in plasma centrifuges.[4–7] Some techniques, mass filters, de-confine particles of a specified mass range. This was first done with a tapered profile of the electric potential that is aimed to only confine light ions radially.[8–11] Maintaining a potential well is also been attempted.[12,13] More recently, a magnetic centrifugal mass filter was built that includes an asymmetrical centrifugal trap that de-confines light and heavy ions at opposite axial ends.[14–17] Radial mass separation that relies on collisions has also been proposed.[18] Yet other techniques stimulate the motion of specific species that are desired to be separated, for example by ionization of specific species by lasers.[19] In all these techniques, the difference in mass results in a difference in particles trajectories, which is used for extracting or filtering out particles of certain range of masses.

Methods that involve electromagnetic waves have also been considered for mass separation. One method is the use of ion cyclotron resonance (ICR),[20–28] where members of the resonant ion-species moving along a uniform magnetic field absorb wave energy and acquire a large perpendicular velocity, which allows separating them from members of the non-resonant ion-species. A second method relies on the ponderomotive force exerted by a standing wave (or a decaying wave) on ions. That ponderomotive force pushes ions along a steady magnetic field in a direction that depends on whether the cyclotron frequency of the ion is larger or smaller than the wave frequency. This method has been explored by Weibel and colleagues[29–31] and also by Ohkawa.[32] The interesting property of the ponderomotive force exerted by a standing wave has been noticed earlier by Motz and Watson.[33]

Our study here of the ponderomotive force exerted by standing waves is motivated by the potential implementation for mass separation. However, there are various difficulties on the way for such an implementation, as we mention later. We, therefore, only examine the basic physical processes involved which we find very interesting. We solve for the ion motion in specified electromagnetic fields and a uniform steady magnetic field. The electromagnetic wave is assumed planar, and all quantities depend on z only, the coordinate along the uniform magnetic field and normal to the wave plane. We show that in a standing wave, ions that their cyclotron frequency is larger than

© Author(s) 2024

the wave frequency tend to move toward and oscillate around the wave magnetic node, while ions of a cyclotron frequency smaller than the wave frequency tend to move toward and oscillate around the wave electric node.

In Sec. II, we solve the ion motion analytically, with the assumption of a small ion axial displacement, both for a traveling wave and a standing wave. Despite the simplifying assumption of a small axial displacement, the analytical result provides, we believe, an insight into the special dynamics due to the ponderomotive force by the standing wave in contrast to traveling wave. The analysis shows that the axial pushing by the ponderomotive force in opposite directions only occurs by a standing wave.

In Sec. III, we extend the analysis to a finite ion axial displacement in a standing wave. The pushing in opposite directions by the ponderomotive force is demonstrated by solving numerically the equations of motion of two lithium isotopes ions, $^6Li^+$ and $^7Li^+$. In Sec. III, we also discuss the possible use of the ponderomotive force for mass separation and the various difficulties in doing that. We compare the pushing by the ponderomotive force to the ICR method.[24–28]

In Secs. IV and V, we examine the dependence of the ion dynamics under the ponderomotive force on the proximity of the wave frequency to the cyclotron frequency. In Sec. IV, we calculate the ion axial velocity upon reaching the wave magnetic node as a function of that proximity. The calculation is made for $^6Li^+$ whose cyclotron frequency is slightly larger than the wave frequency. It is found that as the wave frequency is made closer to the cyclotron frequency, the ion axial velocity at the wave magnetic node first increases. At a certain difference between the frequencies, the ion velocity reaches a maximum. As the wave frequency becomes closer to the cyclotron frequency, the ion axial velocity at the node decreases and finally vanishes at the cyclotron resonance. We analyze this nonmonotonic dependence and derive analytical approximations to this behavior in these two ranges of wave frequencies. The first frequency range is when the wave frequency is less close to the cyclotron frequency. The ion motion can be described by a time-independent potential, the ponderomotive potential.[29] In the second frequency range, when the wave frequency is closer to the ion cyclotron frequency, the ion motion cannot be described by such a ponderomotive potential.

Section V is devoted to the study of the ion dynamics in that second frequency range, very close to the cyclotron resonance, where the description by the ponderomotive potential is not valid. It is shown that the ion performs an oscillatory motion around the wave magnetic node with varying-in-time amplitude and frequency. These oscillations are found to be approximately described by solutions of the Mathieu equation.

II. STANDING VERSUS TRAVELING WAVES NEAR THE CYCLOTRON FREQUENCY

Our aim in this paper is to study the dynamics of ions under the forces by a planar standing wave and a steady uniform magnetic field near the cyclotron resonance. In this section, we compare the ion dynamics under standing waves to the dynamics under traveling waves.

The non-relativistic equations of motion of a particle of mass m and charge q under the forces by the electromagnetic fields $\vec{E}_w$ and $\vec{B}_w$ and a steady uniform magnetic field,

$$\vec{B}_0 = B_0\hat{z}, \quad B_0 > 0, \tag{1}$$

are

$$m\frac{d\vec{v}}{dt} = q\left[\vec{E}_w + \vec{v}\times\left(\vec{B}_w + B_0\hat{z}\right)\right], \quad \frac{dz}{dt} = v_z, \qquad \vec{v}(t=0) = \vec{v}_0, \quad z(t=0) = z_0. \tag{2}$$

Here, $\vec{v}$ is the particle velocity, z is its location, and t is the time. Let us assume a planar standing wave of the form

$$\vec{E}_w = \vec{E}_{sw}(z,t) = E_{sw}(z)\left[\hat{x}\sin(\omega t) + \hat{y}\cos(\omega t)\right], \qquad \vec{B}_w = \vec{B}_{sw}(z,t) = B_{sw}(z)\left[\hat{x}\sin(\omega t) + \hat{y}\cos(\omega t)\right], \tag{3}$$

where

$$B_{sw}(z) = -\frac{1}{\omega}\frac{\partial E_{sw}(z)}{\partial z}. \tag{4}$$

The frequency is positive, $\omega > 0$, so that the wave is left-hand polarized when one looks along the steady uniform magnetic field, at the positive z direction.

In order to demonstrate the importance of the wave being standing wave, we compare the particle dynamics in a standing and in a traveling wave. A planar traveling wave, left-hand polarized with respect to the direction of the steady magnetic field, can be written as

$$\vec{E}_w = \vec{E}_{tw}(z,t) = E_1\left[\hat{x}\cos(\omega t - kz) - \hat{y}\sin(\omega t - kz)\right], \qquad \vec{B}_w = \vec{B}_{tw}(z.t) = B_1\left[\hat{x}\sin(\omega t - kz) + \hat{y}\cos(\omega t - kz)\right], \tag{5}$$

where

$$B_1 = \left(\frac{k}{\omega}\right)E_1. \tag{6}$$

Note that the electric and the magnetic fields of a standing wave are parallel (or anti parallel) to each other, while in a traveling wave, the electric and the magnetic fields are perpendicular to each other.

Let us examine the time dependence of the waves at a certain location, $z = z_0$. We can write Eq. (3) for a standing wave and Eq. (5) for a traveling wave at that specific location in a unified form. The standing wave fields are

$$\vec{E}_{sw}(z_0,t) = E_{sw}(z_0)\left[\hat{x}\cos(\omega t - \pi/2) - \hat{y}\sin(\omega t - \pi/2)\right], \qquad \vec{B}_{sw}(z_0,t) = B_{sw}(z_0)\left[\hat{x}\sin(\omega t) + \hat{y}\cos(\omega t)\right], \tag{7}$$

where

$$B_{sw}(z_0) = -\frac{1}{\omega}\frac{\partial E_{sw}}{\partial z}(z_0). \tag{8}$$

We describe the traveling wave at $z = z_0$ as a function of time, where time is redefined as

$$t(z_0) \equiv t - kz_0/\omega. \tag{9}$$

The traveling wave is then

$$\vec{E}_{tw}(z_0, t(z_0)) = E_1[\hat{x}\cos(\omega t(z_0)) - \hat{y}\sin(\omega t(z_0))], \qquad \vec{B}_{tw}(z_0, t(z_0)) = B_1[\hat{x}\sin(\omega t(z_0)) + \hat{y}\cos(\omega t(z_0))]. \tag{10}$$

A unified form for describing both standing waves [Eq. (7)] and traveling waves [Eq. (10)] at $z = z_0$ is

$$\vec{E}_w(z_0,t) = E_w(z_0)\left[\hat{x}\cos(\omega t - \varphi) - \hat{y}\sin(\omega t - \varphi)\right], \qquad \vec{B}_w(z_0,t) = B_w(z_0)\left[\hat{x}\sin(\omega t) + \hat{y}\cos(\omega t)\right], \tag{11}$$

01 April 2024 17:23:20

© Author(s) 2024

where

$$\varphi = \frac{\pi}{2} \text{ for a standing wave}, \quad \varphi = 0 \text{ for a traveling wave}. \tag{12}$$

We use the same notation t for time for both wave types. $E_w(z_0)$ and $B_w(z_0)$ are related through Eq. (6) for traveling waves and through Eq. (8) for standing waves. For traveling waves, $E_w(z_0)$ and $B_w(z_0)$ are the same for every z_0, while for standing waves they are different for different z_0. The important difference between traveling and standing waves is that in traveling waves the electric and the magnetic fields are perpendicular to each other, while in standing waves the electric field is parallel (or anti-parallel) to the magnetic field.

Equation (11) can be re-written as

$$\vec{E} = E_w\left[\hat{e}_\perp \cos(\varphi) + \hat{e}_\parallel \sin(\varphi)\right], \quad \vec{B} = B_w\hat{e}_\parallel + B_0\hat{z}, \tag{13}$$

where we employ the following system of orthogonal rotating unit vectors $\hat{e}_\perp(t)$, $\hat{e}_\parallel(t)$, and $\hat{z}$,

$$\begin{aligned} \hat{e}_\perp(t) &\equiv \hat{x}\cos(\omega t) - \hat{y}\sin(\omega t), \\ \hat{e}_\parallel(t) &\equiv \hat{x}\sin(\omega t) + \hat{y}\cos(\omega t), \quad \hat{z}. \end{aligned} \tag{14}$$

This system of unit vectors is the same for a specific time at all $z's$ for a standing wave. It is different for at a specific time at different $z's$ for a traveling wave, because of Eq. (9). However, we restrict the comparison of the dynamics under the two types of waves to a small Δz, the axial displacement of the particle,

$$\frac{1}{E_{sw}}\frac{\partial E_{sw}}{\partial z}\Delta z \ll 1, \tag{15}$$

so that along the trajectories the wave fields are time-dependent, but are (approximately) z-independent. We, therefore, solve the equations of motion in the electromagnetic fields described by Eq. (13), where E_w, B_w, and B_0 are taken as z-independent. The rotating unit vector $\hat{e}_\parallel$ points in the direction of the wave magnetic field for both standing and traveling waves, while $\hat{e}_\perp$ is perpendicular to the magnetic field. In a traveling wave, the wave electric field is parallel to $\hat{e}_\perp$, while in a standing wave the wave electric field is parallel to the magnetic field, and parallel to $\hat{e}_\parallel$ as well.

Writing the particle velocity as $\vec{v} = v_\perp\hat{e}_\perp + v_\parallel\hat{e}_\parallel + v_z\hat{z}$, and noticing that

$$\frac{d\hat{e}_\perp(t)}{dt} = -\hat{e}_\parallel(t), \quad \frac{d\hat{e}_\parallel(t)}{dt} = \hat{e}_\perp(t), \tag{16}$$

we write the equations of motion, under the assumption (15), as

$$\begin{aligned} &\frac{dv_\perp}{dt} - (\omega_0 - \omega)v_\parallel + \omega_1 v_z = a\cos(\varphi), \\ &\frac{dv_\parallel}{dt} + (\omega_0 - \omega)v_\perp = a\sin(\varphi), \quad \frac{dv_z}{dt} - \omega_1 v_\perp = 0, \\ &\vec{v}(t=0) = (v_{\perp 0}, v_{\parallel 0}, v_{z0}), \quad z \cong z(t=0) = z_0, \end{aligned} \tag{17}$$

where

$$a \equiv \frac{qE_w}{m}, \quad \omega_0 \equiv \frac{eB_0}{m}, \quad \omega_1 \equiv \frac{qB_w}{m}. \tag{18}$$

Here, a and ω_1 are also approximated as constants, following Eq. (15). The analytical solution of the equations of motion (17) is then

$$\begin{aligned} v_\perp = {} & v_{\perp 0}\cos(\Omega t) + \left[v_{\parallel 0}\frac{(\omega_0 - \omega)}{\Omega} - v_{z0}\frac{\omega_1}{\Omega}\right]\sin(\Omega t) \\ & + \cos\varphi\frac{a}{\Omega}\sin(\Omega t) + \sin\varphi\frac{a}{\Omega}\frac{(\omega_0 - \omega)}{\Omega}[1 - \cos(\Omega t)], \end{aligned} \tag{19}$$

$$\begin{aligned} v_\parallel = {} & -v_{\perp 0}\frac{(\omega_0 - \omega)}{\Omega}\sin(\Omega t) + v_{\parallel 0}\left[\frac{(\omega_0 - \omega)^2}{\Omega^2}\cos(\Omega t) + \frac{\omega_1^2}{\Omega^2}\right] \\ & + v_{z0}\frac{\omega_1(\omega_0 - \omega)}{\Omega^2}[1 - \cos(\Omega t)] \\ & - \cos\varphi\frac{a}{\Omega}\frac{(\omega_0 - \omega)}{\Omega}[1 - \cos(\Omega t)] \\ & + \sin\varphi\frac{a}{\Omega}\left[\frac{\omega_1^2}{\Omega^2}\Omega t + \frac{(\omega_0 - \omega)^2}{\Omega^2}\sin(\Omega t)\right], \end{aligned} \tag{20}$$

$$\begin{aligned} v_z = {} & v_{\perp 0}\frac{\omega_1}{\Omega}\sin(\Omega t) + v_{\parallel 0}\frac{\omega_1(\omega_0 - \omega)}{\Omega^2}[1 - \cos(\Omega t)] \\ & + v_{z0}\left[\frac{(\omega_0 - \omega)^2}{\Omega^2} + \frac{\omega_1^2}{\Omega^2}\cos(\Omega t)\right] \\ & + \cos\varphi\frac{a}{\Omega}\frac{\omega_1}{\Omega}[1 - \cos(\Omega t)] \\ & + \sin\varphi\frac{a}{\Omega}\frac{\omega_1(\omega_0 - \omega)}{\Omega^2}[\Omega t - \sin(\Omega t)]. \end{aligned} \tag{21}$$

Here,

$$\Omega^2 \equiv (\omega_0 - \omega)^2 + \omega_1^2. \tag{22}$$

The singularity at the cyclotron frequency is resolved here by the wave magnetic field B_w having a finite value.

It is seen in Eq. (21) that in a standing wave ($\sin\varphi = 1$), the particle axial velocity grows linearly in time (when $\Omega t > \pi/2$) as expressed by the secular term. Moreover, the direction of that increasing velocity depends on the sign of $\omega_0 - \omega$. A particle is pushed in one z direction if

$$\omega_0 > \omega, \tag{23}$$

and it is pushed in the opposite z direction if $\omega_0 < \omega$. Thus, the force exerted by a standing wave can push two ions that differ in ω_0 (due to their different mass) in opposite axial directions, what leads to mass separation. This property is unique to standing waves. In contrast, in a traveling wave ($\cos\varphi = 1$), there is no secular term in the expression for v_z, and all ions are pushed in the same axial direction irrespective of their mass.

It should be noted that the axial pushing is second order in the wave fields. It is proportional to the product of the wave electric field (a) by the wave magnetic field (ω_1). In contrast, ICR, the ion cyclotron resonance heating,[20] is first-order in the wave fields. Within our expression, ion cyclotron resonance heating is described by the first term in the expression for $v_\parallel$, the velocity component parallel to the wave electric field. Exactly at resonance, $v_\parallel = at = (qE_w/m)t$, and this linear-in-time increase in $v_\parallel$ is proportional to the wave electric field a only; the increase occurs even if the wave magnetic field is zero, $\omega_1 = 0$. Ion cyclotron resonance is being explored for mass separation in Kurchatov.[24–28] For mass separation, a uniform steady magnetic field is used, which is different from the narrow resonant layer along a nonuniform steady magnetic field which is used for ICRH in magnetic fusion configurations.[34–36] The two methods for mass separation, ICR and the axial pushing presented here, will be compared later in this paper.

01 April 2024 17:23:20

© Author(s) 2024

We demonstrated the possibility of standing waves of a frequency near the cyclotron frequency causing mass separation through opposite axial pushing. The analysis did not consider the spatial variation of the wave. In Sec. III, we examine numerically the dynamics in standing waves with the spatial dependence of the wave.

III. STANDING WAVES NEAR THE ION CYCLOTRON FREQUENCY

In the rest of this paper, we only address the dynamics understanding waves. We choose to substitute into Eq. (3) the quantities,

$$\begin{aligned} E_{sw}(z) &= \sqrt{2}E_1 \sin(kz+\pi/4), \\ B_{sw}(z) &= \sqrt{2}B_1 \cos(kz+\pi/4), \quad B_1 = \frac{k}{\omega}E_1. \end{aligned} \tag{24}$$

This form of the coefficients is chosen for convenience, since we intend to integrate the equations from $z=0$, preferring that at that initial position the electric and magnetic fields are both not too small (at $z=0$ both fields are $1/\sqrt{2}$ of their maximal values). An analysis for ions who start their motion from rest at $z \neq 0$ is not done here, although it is expected to be qualitatively similar. The standing wave is, therefore, of the form

$$\begin{aligned} \vec{E}_w &= \vec{E}_{sw}(z,t) = \sqrt{2}E_1 \sin(kz+\pi/4)\left[\hat{x}\sin(\omega t)+\hat{y}\cos(\omega t)\right], \\ \vec{B}_w &= \vec{B}_{sw}(z,t) = \sqrt{2}B_1 \cos(kz+\pi/4)\left[\hat{x}\sin(\omega t)+\hat{y}\cos(\omega t)\right], \\ B_1 &= \frac{k}{\omega}E_1. \end{aligned} \tag{25}$$

The electric field and the magnetic field are parallel to each other. Such a standing wave is generated in the standard way by launching two counter-propagating traveling waves: one propagates in the positive z direction,

$$\begin{aligned} \vec{E}_+(z,t) &= \frac{E_1}{\sqrt{2}}\left[\hat{x}\cos\left(\omega t-kz-\frac{\pi}{4}\right)-\hat{y}\sin\left(\omega t-kz-\frac{\pi}{4}\right)\right], \\ \vec{B}_+(z,t) &= \frac{B_1}{\sqrt{2}}\left[\hat{x}\sin\left(\omega t-kz-\frac{\pi}{4}\right)+\hat{y}\cos\left(\omega t-kz-\frac{\pi}{4}\right)\right], \end{aligned} \tag{26}$$

and the second propagates in the negative z direction,

$$\begin{aligned} \vec{E}_-(z,t) &= \frac{E_1}{\sqrt{2}}\left[-\hat{x}\cos\left(\omega t+kz+\frac{\pi}{4}\right)+\hat{y}\sin\left(\omega t+kz+\frac{\pi}{4}\right)\right], \\ \vec{B}_-(z,t) &= \frac{B_1}{\sqrt{2}}\left[\hat{x}\sin\left(\omega t+kz+\frac{\pi}{4}\right)+\hat{y}\cos\left(\omega t+kz+\frac{\pi}{4}\right)\right]. \end{aligned} \tag{27}$$

Both counter-propagating traveling waves are left-hand polarized when looking in the positive z direction (the wave that propagates in the negative z direction is right-hand polarized with respect to its direction of propagation).

Using the unit vectors [Eq. (14)] and Eq. (13), we write the equations of motion, Eq. (2), as

$$\begin{aligned} m\frac{d\vec{v}}{dt} &= q\Big[\sqrt{2}E_1 \sin(kz+\pi/4)\hat{e}_\parallel \\ &\quad + \vec{v}\left(\sqrt{2}B_1\cos(kz+\pi/4)\hat{e}_\parallel + B_0\hat{z}\right)\Big], \\ \frac{dz}{dt} &= v_z, \quad \vec{v}(t=0)=\vec{v}_0, \quad z(t=0)=z_0. \end{aligned} \tag{28}$$

Note that we consider standing waves for which $\sin\varphi = 1$. The equations for the components of the particle velocity, Eqs. (17), become

$$\begin{aligned} \frac{dv_\perp}{dt} - (\omega_0-\omega)v_\parallel + \sqrt{2}\omega_{10}\cos(kz+\pi/4)v_z &= 0, \\ \frac{dv_\parallel}{dt} + (\omega_0-\omega)v_\perp &= \sqrt{2}a_0\sin(kz+\pi/4), \\ \frac{dv_z}{dt} - \sqrt{2}\omega_{10}\cos(kz+\pi/4)v_\perp &= 0, \\ \frac{dz}{dt} = v_z, \quad \vec{v}(t=0) = (v_{\perp 0}, v_{\parallel 0}, v_{z0}), &\quad z(t=0)=z_0, \end{aligned} \tag{29}$$

where

$$a_0 \equiv \frac{qE_1}{m}, \quad \omega_0 \equiv \frac{eB_0}{m}, \quad \omega_{10} \equiv \frac{qB_1}{m}, \quad B_1 = \frac{k}{\omega}E_1. \tag{30}$$

The approximation described in Sec. II, valid when Eq. (15) holds, holds in the particular form described by Eq. (24) when

$$k\Delta z \ll \frac{\pi}{2} \tag{31}$$

holds. The analytical solution near $z=0$, Eqs. (19)–(21), reduce, when $\vec{v}_0 = 0$, to

$$\begin{aligned} v_\perp &= \frac{a_0}{\Omega}\frac{(\omega_0-\omega)}{\Omega}[1-\cos(\Omega t)], \\ v_\parallel &= \frac{a_0}{\Omega}\left[\frac{\omega_{10}^2}{\Omega^2}\Omega t + \frac{(\omega_0-\omega)^2}{\Omega^2}\sin(\Omega t)\right], \\ v_z &= \frac{a_0}{\Omega}\frac{\omega_{10}(\omega_0-\omega)}{\Omega^2}[\Omega t - \sin(\Omega t)]. \end{aligned} \tag{32}$$

As is written in Sec. II, it is seen that there is an axial acceleration due to the secular term in the expression for v_z. The direction of the resulting axial velocity v_z is positive for $\omega_0-\omega>0$ and is negative for $\omega_0-\omega<0$. The axial acceleration vanishes at the cyclotron frequency. These directions correspond to

$$a_0 > 0, \quad \omega_{10} > 0, \tag{33}$$

or to $E_1>0$, $B_1>0$. If one of these quantities becomes negative, the direction of acceleration reverses. The axial displacement within the assumption (31) is

$$z = \int_0^t v_z dt' = \frac{a}{\Omega}\frac{\omega_{10}(\omega_0-\omega)}{\Omega^3}\left[\frac{\Omega^2 t^2}{2}+\cos(\Omega t)-1\right]. \tag{34}$$

Figure 1 shows the electric and magnetic fields of a standing wave as in Eq. (24), where the electric field is $E_1 = 50\,\mathrm{V/m}$ (the maximal electric field is $\sqrt{2}\times 50\,\mathrm{V/m}$) and the wavelength is $\lambda = 4\,\mathrm{m}$ ($k = 2\pi/\lambda$). The arrows in green show the direction of the force on ions, the cyclotron frequency of which is larger than the wave frequency, while the arrows in yellow show the direction of force on ions, the cyclotron frequency of which is smaller than the wave frequency. The direction of the force will be discussed shortly.

Figure 2 shows the axial velocity v_z along the particle trajectory for the $^6Li^+$ and of $^7Li^+$ ions, both released at rest at $z=0$, under the forces by these wave fields and by a steady magnetic field of $B_0 = 2\,\mathrm{kG}$. The velocity is obtained as a solution of Eq. (29) with $\vec{v}(t=0) = 0$, $z(t=0)=0$. The wave frequency is $\omega = \omega_f$, the average of their

01 April 2024 17:23:20

© Author(s) 2024

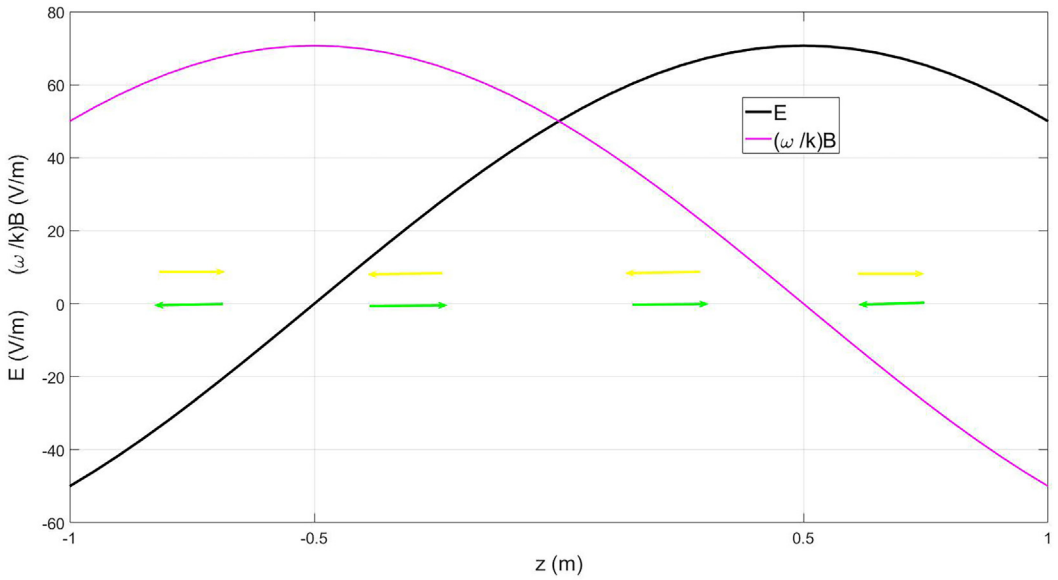

FIG. 1. The electric field and the magnetic field of the standing wave as in Eq. (24): $E_1 = 50\,\mathrm{V/m}$, $k = \pi/(2\,\mathrm{m})$. The arrows show the direction of the force on ions, the cyclotron frequency of which is larger (green) or smaller (yellow) than the wave frequency. These wave fields were used for all the figures (together with $B_0 = 2\,\mathrm{kG}$).

corresponding cyclotron frequencies, $\omega_{0,6} = 3.193 \times 10^6\,\mathrm{s}^{-1}$ and $\omega_{0,7} = 2.737 \times 10^6\,\mathrm{s}^{-1}$,

$$\omega_f \equiv \frac{\omega_{0,6} + \omega_{0,7}}{2} = 2.965 \times 10^6\,\mathrm{s}^{-1}. \tag{35}$$

The phase velocity $v_{ph}(\equiv \omega/k) \cong 2 \times 10^6\,\mathrm{m/s}$ is much smaller than the speed of light in vacuum. An appropriate plasma medium is needed for that, which we do not discuss here. For that phase velocity, the wave magnetic field is $B_1 = 2.5 \times 10^{-5}\,\mathrm{T}$. It is shown in Fig. 2 that initially $^6\mathrm{Li}^+$ is accelerated to the right, while $^7\mathrm{Li}^+$ is accelerated to the left. In Fig. 2 shown are also the analytic approximate solutions, Eqs. (32) and (34), calculated for the wave parameters at $z = 0$. The analytic solutions deviate from the numerical solution as the wave electric and magnetic fields change along the trajectories.

As the ions reach either $z = 0.5$ or $z = -0.5\,\mathrm{m}$ ($\lambda/8 = \pi/4k = 0.5\,\mathrm{m}$), the direction of the force is reversed. Accordingly, the two

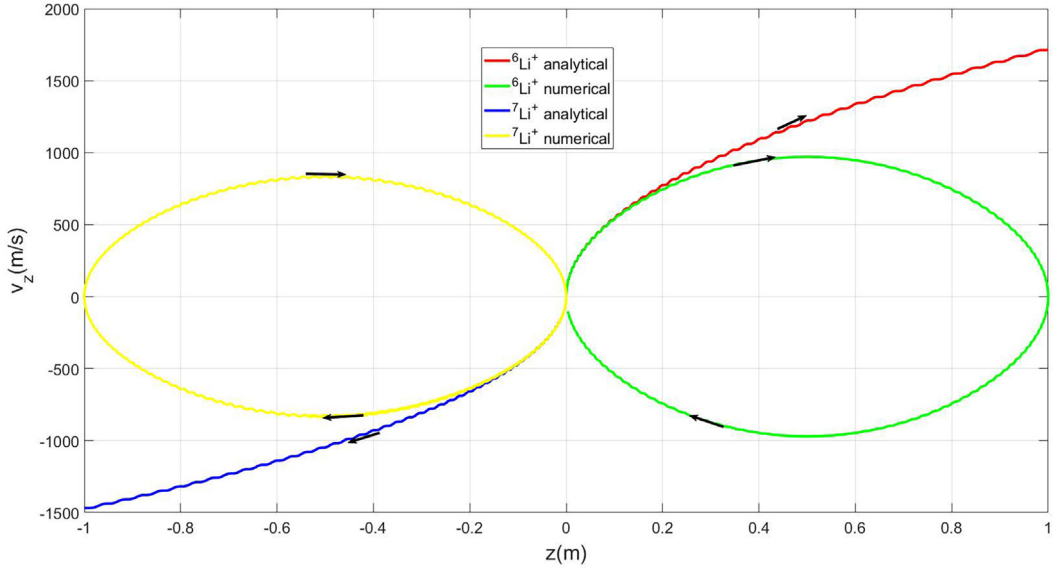

FIG. 2. $^6\mathrm{Li}^+$ and $^7\mathrm{Li}^+$ axial velocities along z, under the fields of Fig. 1: $\omega = \omega_f = (\omega_{0,6} + \omega_{0,7})/2$. The particles perform periodic orbits in opposite directions. The analytic calculations describe well the ions motion at earlier times. Collisions, self-fields, and radial gradients are neglected in all the calculations.

01 April 2024 17:23:20

© Author(s) 2024

ions each perform periodic orbits. The force reversal occurs when either the wave electric field or wave magnetic field changes its sign, at the node of either of them. We will later examine the periodic motion of the ions around the wave magnetic field node. However, for mass separation it is desirable to collect the ions at the end of uni-directional acceleration, at either node, here at $z = \pm 0.5$ m.

Figure 3 shows the trajectories of the two lithium isotopes from $z = 0$ until they reach the wave nodes either at $z = 0.5$ or $z = -0.5$ m. The radial excursion of the ions along their trajectory is few mm only.

A. Implementation for mass separation

In order to achieve high throughput, the process of mass separation has to be realized in a plasma. The plasma is also a medium appropriate to support waves with a low phase velocity (probably the shear-Alfvén wave). Ways to introduce appropriate electromagnetic fields into the plasma have to be employed. In addition to this challenge, electrostatic space-charge fields of the plasma that also affect the plasma dynamics have to be considered. Collisions, plasma pressure, and self-fields of the plasma may blur the effect and weaken the mass separation process. Some of these effects probably interfere with processes that are used in other methods, such as the ICR, that is nevertheless successful in demonstrating mass separation.[24–28] The ICR has a clear advantage relative to the ponderomotive force in that it relies on a process that is first order in the wave field (the magnetic field of the wave does not play any role in the ICR). The ponderomotive force is second order in the wave fields—it is proportional to the product of the wave electric and magnetic fields. The ponderomotive force is, therefore, weaker, the ions gain a low velocity in this configuration, and the process is more vulnerable to the effects mentioned above.

A requirement that is common to both methods for mass separation, ICR and the ponderomotive force, is that the steady magnetic field is uniform and that the wave frequency is accurately close to the cyclotron frequency. In the ICR method, the wave frequency and the magnetic field intensity should be arranged with sufficient accuracy so that one of the two ions to be separated only be heated. When the ponderomotive force is used, both ions could be close to the resonance, because the resonance affect both in the desirable way, pushing them in opposite directions.

Another important issue is the collection of the separated ions. When ICR is used, all ions flow in the same direction and the separation is realized by collecting specifically the resonant ion species which acquires a large perpendicular velocity. In contrast, the process studied here has the advantage that the separated ions are pushed by the ponderomotive force in opposite directions, thus the ions are separated in space. The pushed ions should be collected at the wave nodes. The collection at the wave electric node can be made by placing a reflecting metal surface there. The metal surface reflects the electromagnetic wave, and the electric node is formed naturally. $^{7}Li^{+}$ ions in our example can be collected by the reflecting surface, which is at the wave electric node. More difficult is collecting the light ions, $^{6}Li^{+}$ in our case, at the magnetic node. The positioning of an appropriate antenna and a collecting surface, so that they do not interfere, is the challenge here. This difficulty motivated us to examine the ion dynamics near the wave magnetic node.

In summary, the main advantage of ICR relative to the ponderomotive force for mass separation is that ICR is first order in the wave fields, while the ponderomotive force is second-order in the wave fields. Therefore, the ponderomotive force is weaker. The advantage of the ponderomotive force is that it separates ions in space and it does not rely on the difference in energy between ions. The challenge is to devise a configuration in which the ponderomotive force is larger, so that the separation effect is not blurred by other effects.

In Sec. IV, we examine the effect of the proximity to the cyclotron resonance on the axial velocity that is reached at the wave magnetic field node.

IV. THE AXIAL VELOCITY AND THE PROXIMITY TO THE CYCLOTRON RESONANCE

We calculate here the axial velocity v_z of $^{6}Li^{+}$ ion that is released at rest at $z = 0$, upon reaching for the first time the wave magnetic field node at $z = 0.5$ m, for different values of ω at the neighborhood of $\omega_{0.6}$. Except for ω, which is varied, all the parameters are as in Sec. III. The ion motion of a cyclotron frequency smaller than the wave frequency near the wave electric node (here $^{7}Li^{+}$ ion axial velocity at $z = -0.5$ m) will be examined in a future study.

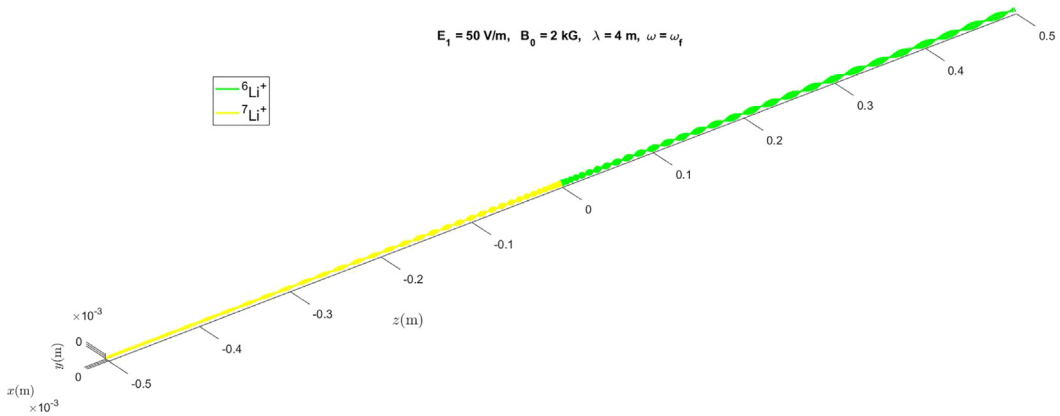

FIG. 3. $^{6}Li^{+}$ and $^{7}Li^{+}$ trajectories under the fields of Fig. 1 and with $\omega = \omega_f$.

01 April 2024 17:23:20

© Author(s) 2024

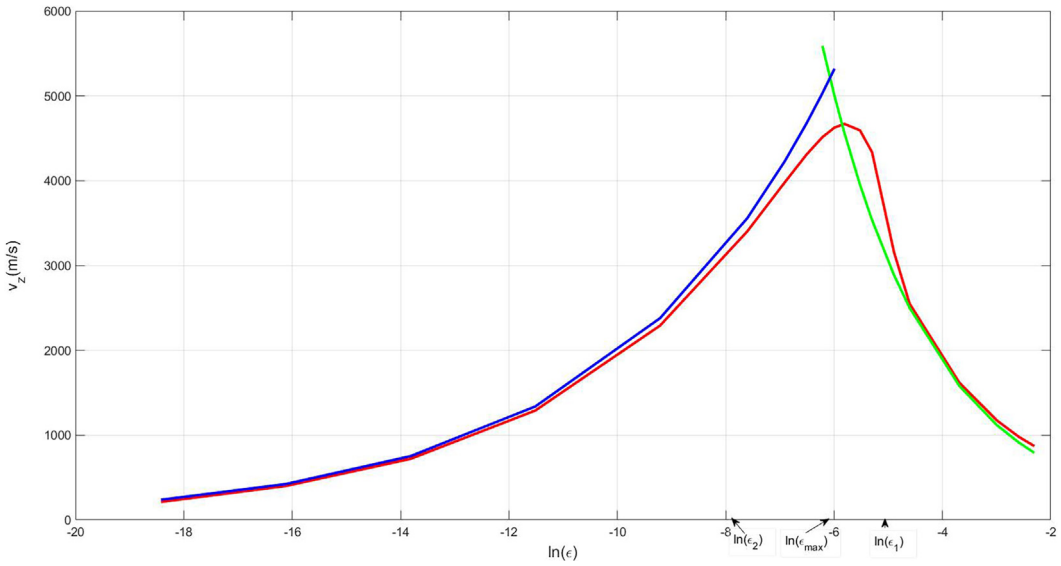

FIG. 4. The axial velocity of $^6Li^+$ that is released at rest at $z=0$ when it reaches for the first time the wave magnetic node at $z=0.5$ m, as a function of $\ln(\epsilon)$; $\epsilon=\omega_{0,6}/\omega-1$. The numerical solution of Eq. (29) is shown in red, the approximate solution [Eq. (48)] in green, and the approximate solution [Eq. (53)] in blue. Also shown are the locations of ϵ_1, ϵ_2, and ϵ_{max}.

Figure 4 shows the axial velocity v_z of $^6Li^+$ ion that is released at rest at $z=0$, upon reaching the wave magnetic field node at $z=0.5$ m, as a function of $\ln\epsilon$, where

$$\epsilon\equiv\frac{\omega_{0,6}}{\omega}-1. \tag{36}$$

The nonmonotonic red line shows the results of a numerical solution of Eq. (29). On the right side of the figure, ϵ is larger, while on the left side of the figure, ϵ is smaller. It is seen in the figure that as ω gets closer to the resonance (ϵ gets smaller), the axial velocity v_z at the node becomes larger, and reaches a maximal value ($v_{z,\max}\cong 4500$ m/s) at $\epsilon=\epsilon_{\max}\cong 0.003$ ($\omega\cong 3.183\times10^6$ s^{-1}). When ω is closer to the resonance, ϵ gets further smaller, v_z at the node becomes smaller, reaching zero at resonance ($v_z=0$ at $\epsilon=0$). As mentioned above, we note that in practice it is hard to maintain either ω or B_0 to such accuracy, so that ϵ is controlled, but we nevertheless study this dependence, for its interest as basic physics. We also note that the results here are valid for ions which start their motion at $z=0$. The behavior of ions which start their motion at other axial locations between the same magnetic and electric nodes ($z=0.5$ and $z=-0.5$ m) is expected to be qualitatively similar.

In order to understand the dependence shown in Fig. 4, we examine Eq. (29). We first assume that

$$(\omega_{0,6}-\omega)v_\parallel\gg\sqrt{2}\omega_{10}\cos(kz+\pi/4)v_z,$$

so that we neglect the third term on the left side of the first of Eqs. (29). This is equivalent to approximating

$$\Omega=|\omega_0-\omega|=\epsilon\omega, \tag{37}$$

in Eq. (32). The equations for $v_\perp$ and $v_\parallel$ are combined to

$$\frac{d(v_\perp+iv_\parallel)}{dt}+i\epsilon\omega(v_\perp+iv_\parallel)=i\sqrt{2}a_0\sin(kz+\pi/4), \tag{38}$$

the solution of which is

$$v_\perp+iv_\parallel=i\sqrt{2}a_0\int_0^t\exp\left[i\epsilon\omega(t'-t)\right]\sin\left[kz(t')+\pi/4\right]dt'. \tag{39}$$

Thus,

$$v_\perp=\sqrt{2}a_0\int_0^t\sin\left[\epsilon\omega(t-t')\right]\sin\left[kz(t')+\pi/4\right]dt'. \tag{40}$$

Integration by parts yields

$$v_\perp=\frac{\sqrt{2}v_q}{\epsilon}\left\{\sin\left[kz(t)+\pi/4\right]-\sin(\pi/4)\cos(i\epsilon\,\omega t)+\int_0^t\cos\left[i\epsilon\omega(t-t')\right]kv_z(t')\cos\left[kz(t')+\pi/4\right]dt'\right\}. \tag{41}$$

Here,

$$v_q\equiv\frac{a_0}{\omega} \tag{42}$$

is the quiver velocity. For our choice of parameters, the quiver velocity near the $^6Li^+$ cyclotron resonance is $v_q\cong 250$ m/s.

We now discuss separately the cases in which the oscillatory part in the expression for $v_\perp$ can and cannot be neglected.

A. The ponderomotive potential regime

Let us assume that the transit time, the time $t(z=\pi/4k)$ it takes for the ion to reach the node at $z=\lambda/8=\pi/4k$, satisfies

$$\epsilon\omega t(z=\pi/4k)>2\pi. \tag{43}$$

This regime is characterized by a long-enough transit time $[t(z=\pi/4k)]$. We then neglect the oscillating-in-time terms, so that

01 April 2024 17:23:20

© Author(s) 2024

$$v_\perp = \frac{\sqrt{2}}{\epsilon} v_q \sin\left[kz(t) + \pi/4\right]. \tag{44}$$

Note that $v_\perp$, as expressed in (44), is the average value of the oscillatory solution.

From Eq. (29), we find that

$$\frac{dv_z}{dt} - \frac{v_{q^2}}{\epsilon}\frac{d}{dz}\left[\sin^2(kz + \pi/4)\right] = 0,$$

where $\omega_{10} = (k/\omega)a_0$ [Eq. (30)] is used. We can define in this regime the ponderomotive force exerted by the standing wave as the gradient of a ponderomotive potential,[29] a form that is valid not too close to the cyclotron resonance. In our formalism, we define the ponderomotive force $f_{pm,6}$ and the associated ponderomotive potential $\varphi_{pm,6}$ as

$$\begin{aligned} f_{pm,6} &\equiv -\frac{\partial}{\partial z}\varphi_{pm,6}, \\ \varphi_{pm,6} &\equiv -\frac{mv_q^2}{2\epsilon}\left[\sin^2(kz + \pi/4) - 0.5\right] = -\frac{mv_q^2}{2\epsilon}\sin(2kz). \end{aligned} \tag{45}$$

We chose the ponderomotive potential to be zero at $z = 0$. With the relation $d/dt = v_z d/dz$, the ion axial kinetic energy, $E_{Kz,6} \equiv mv_{z,6}^2/2$, should satisfy

$$E_{Kz,6} + \varphi_{pm,6} = \text{const}. \tag{46}$$

Since we assume that the axial velocity at $z = 0$ is zero, the axial velocity satisfies

$$v_{z,6}^2 = \frac{v_q^2}{\epsilon}\sin(2kz). \tag{47}$$

The axial velocity at the node at $z = \lambda/8 = \pi/4k$ is

$$v_{z,6}\left(z = \frac{\pi}{4k}\right) = \frac{v_q}{\sqrt{\epsilon}}. \tag{48}$$

The green line in Fig. 4 shows the expression in (48). It is a good approximation for the larger values of ϵ to the red line that shows $v_{z,6}(z = \pi/4k)$ as the numerical solution of Eq. (29).

The time it takes for the ion to reach the node is found to be

$$\omega t(z = \pi/4k) = \frac{1}{2}\frac{v_{ph}}{v_q}\sqrt{\epsilon}\int_0^{\pi/2}\frac{ds}{\sqrt{\sin s}} = 1.31\frac{v_{ph}}{v_q}\sqrt{\epsilon}.$$

The requirement that the oscillatory term can be neglected, Eq. (43), becomes, in terms of ϵ

$$\epsilon > \epsilon_1 \equiv 2.84\left(\frac{v_q}{v_{ph}}\right)^{2/3}. \tag{49}$$

For our parameters

$$\epsilon_1 = 0.007, \quad \ln(\epsilon_1) = -5. \tag{50}$$

Indeed, in Fig. 4, the green line deviates from the numerical calculation when $\epsilon \cong \epsilon_1$.

We note that using Eq. (32), we can obtain an expression for $v_{z,6}^2(z = \pi/4k)$, which is a good approximation to Eq. (48). For that, we neglect the oscillatory term in the expression for v_z in Eq. (32), assuming that $\Omega \cong \epsilon\omega$ and $\Omega t \cong \epsilon\omega t(z = \pi/4k) > 2\pi$, so that Eq. (43) holds. Equation (32) expresses a constant axial acceleration. The value of $v_{z,6}(z = \pi/4k)$ is then found to be $\sqrt{\pi/2}$ larger than in Eq. (48), the overestimate is due to the neglect of the spatial dependence of the wave fields.

B. The non-conservative regime

We turn to the case of smaller ϵ, in order to understand the decrease in $v_z(z = \pi/4k)$ when ϵ decreases, as seen on the left side of Fig. 4. We discuss here the velocity of $^6Li^+$ only. When ϵ is small enough, the oscillatory-in-time term in Eq. (41) cannot be neglected. The approximate expression (48) does not hold any more. Instead, we use the spatially independent expression for v_z in Eq. (32) where now we approximate

$$\Omega t \ll 1, \quad \Omega t - \sin(\Omega t) \cong \frac{1}{6}(\Omega t)^3; \quad v_z = \epsilon b\frac{v_q^2}{6v_{ph}}\tau^3; \quad \tau \equiv \omega t. \tag{51}$$

Again, we substituted $\omega_{10} = a_0/v_{ph}$ ($v_{ph} = \omega/k$). We often use the dimensionless time, $\tau \equiv \omega t$, in the expressions and also in the figures. We added a numerical factor b to compensate for the spatially varying wave fields. The time it takes for a particle to reach z is $t = [24zv_{ph}/bv_q^2\omega^3\epsilon]^{1/4}$, so that at the node, at $z = \pi/4k$, the time is

$$\tau = \left(\frac{v_{ph}}{v_q}\right)^{1/2}\left(\frac{6\pi}{b\epsilon}\right)^{1/4}. \tag{52}$$

From Eqs. (51) and (52), we find that at the node ($z = \pi/4k$), the velocity is

$$v_z = \left(\frac{b\pi^3}{6}\right)^{1/4}(v_q v_{ph})^{1/2}\epsilon^{1/4}. \tag{53}$$

When we choose $b^{1/4} = 0.7$, the approximate expression denoted in Fig. 4 by the blue line agrees well with the numerical solution denoted by the red line for

$$\epsilon\tau(z = \pi/4k) < \frac{\pi}{4}. \tag{54}$$

The non-conservative regime is characterized by a short (here normalized) transit time. Using Eq. (52), we obtain the condition

$$\epsilon < \epsilon_2 = \frac{(\pi/4)^{4/3}b^{1/3}}{(6\pi)^{1/3}}\left(\frac{v_q}{v_{ph}}\right)^{2/3}. \tag{55}$$

For the parameters in Fig. 4,

$$\epsilon_2 = 4.2 \times 10^{-4}, \quad \ln(\epsilon_2) = -7.8. \tag{56}$$

These limiting values ϵ_1 and ϵ_2 for the two approximate regimes are denoted in Fig. 4.

C. Estimate of the maximal velocity

The maximal velocity can be roughly estimated by the value of the velocity at the intersection of the green and the blue lines expressing Eqs. (48) and (53). Equating these two expressions, we find ϵ_{max}, the approximate value of ϵ at which the axial velocity is maximal, and the approximated maximal velocity as

01 April 2024 17:23:20

© Author(s) 2024

$$\epsilon_{\max} = \frac{1}{b^{1/3}}\left(\frac{6}{\pi^3}\right)^{1/3}\left(\frac{v_q}{v_{ph}}\right)^{2/3} = 0.0023, \quad \ln(\epsilon_{\max}) = -6.1,$$
$$v_{z,\max} = b^{1/6}\left(\frac{\pi^3}{6}\right)^{1/6}\left(v_q^2 v_{ph}\right)^{1/3} = 5180\,\mathrm{ms}^{-1}. \tag{57}$$

The velocity calculated within this approximation is larger than the velocity 4500 ms^{-1} that is found numerically.

V. OSCILLATORY SOLUTIONS

Ions that cross the nodes at $z = \pm\pi/4k = \pm 0.5$ m feel a force that opposes their motion, thus the ions exhibit an oscillatory motion around the node. We treat separately the ponderomotive potential regime and the non-conservative regime.

A. The ponderomotive potential regime

We analyze the case of $\omega = \omega_f$ [Eq. (35)], for which $\epsilon = 0.077$, so that the conditions for the case addressed in Sec. IV A hold, for both $^6Li^+$ and $^7Li^+$. The ponderomotive force and the ponderomotive potential for $^7Li^+$ are written, similarly to Eq. (45), as

$$f_{pm,7} \equiv -\frac{\partial}{\partial z}\varphi_{pm,7};$$
$$\varphi_{pm,7} \equiv -\frac{ma_0^2}{\omega(\omega_{0,7}-\omega)}\left[\sin^2(kz+\pi/4) - 0.5\right] = \frac{mv_q^2}{2\epsilon}\sin(2kz). \tag{58}$$

When $\omega = \omega_f$, we obtain $\omega_{0,7} - \omega = \omega - \omega_{0,6} = -\epsilon$.

Figure 5 shows the ponderomotive potential, the axial kinetic energy, and their sum for the two ions, $^6Li^+$ and $^7Li^+$, when $\omega = \omega_f$. We note that φ_{pm} is different for the two ions. The frequency is far enough from the cyclotron frequency, and, indeed, as is seen in the figure, energy is conserved for the two ions, in the context of Eq. (46) being satisfied.

B. The non-conservative regime

The non-conservative mode is studied, as earlier, for the velocity of $^6Li^+$ only while this ion moves toward and oscillates around the wave magnetic node. We examine the oscillatory solutions for $\epsilon < \epsilon_2$, and, for the numerical calculation, we choose $\epsilon = 10^{-5}$. Practically, it is difficult to maintain either the steady magnetic field or the wave frequency uniform to such accuracy. In Eq. (29), we again neglect the term $\sqrt{2}\omega_{10}\cos(kz+\pi/4)v_z$ in the equation for $v_\perp$. At the neighborhood of the node, $z \simeq \pi/4k$, we approximate

$$\sin(kz+\pi/4) \simeq 1, \quad \cos(kz+\pi/4) \simeq -k\xi, \quad \xi \equiv z - \frac{\pi}{4k}, \tag{59}$$

where

$$|\xi| \ll \frac{\pi}{4k}. \tag{60}$$

The approximated equations are

$$\frac{dv_\perp}{d\tau} - \epsilon v_\parallel = 0, \quad \frac{dv_\parallel}{d\tau} + \epsilon v_\perp = \sqrt{2}v_q,$$
$$\frac{dv_z}{d\tau} + \sqrt{2}\frac{v_q}{v_{ph}}k\xi v_\perp = 0, \quad \frac{d(k\xi)}{d\tau} = \frac{v_z}{v_{ph}}. \tag{61}$$

The perpendicular velocity is expected to grow-in-time to much larger values than its initial values while the particle first crosses the wave magnetic node. We, therefore, approximate $v_\perp(0) \cong 0$, $v_\parallel(0) \cong 0$, and obtain

$$v_\perp = \frac{\sqrt{2}v_q}{\epsilon}[1-\cos(\epsilon\tau)]; \quad v_\parallel = \frac{\sqrt{2}v_q}{\epsilon}\sin(\epsilon\tau). \tag{62}$$

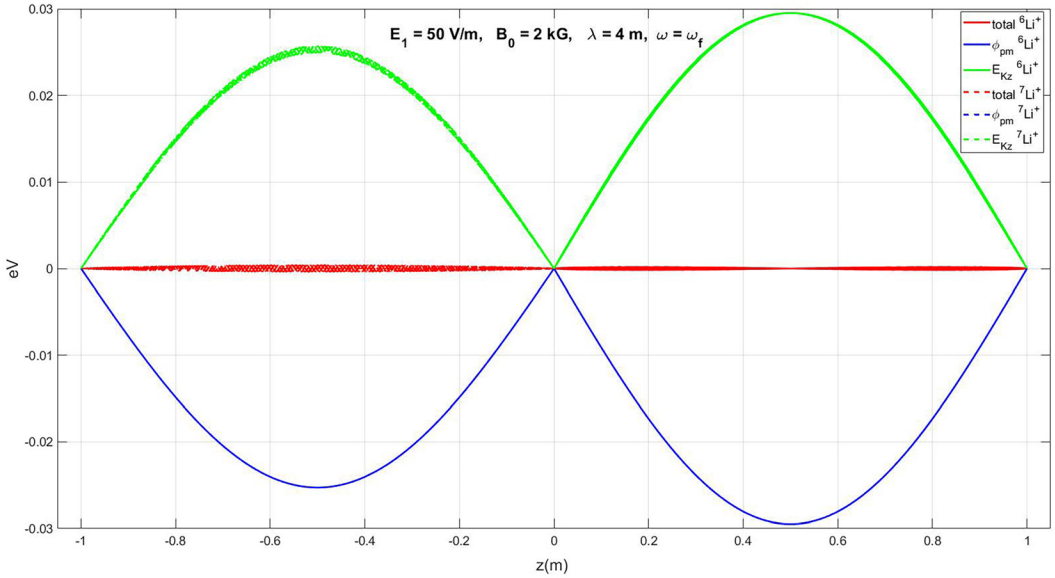

FIG. 5. The axial kinetic energy, the ponderomotive potential, and their sum, the total energy, for $^6Li^+$ and $^7Li^+$ under the fields of Fig. 1, $\omega = \omega_f$ ($\epsilon = 0.077$). The sum is constant expressing energy conservation during the periodic motion.

01 April 2024 17:23:20

© Author(s) 2024

The numerically calculated velocities are very close to the expressions (62). The total perpendicular velocity is

$$\sqrt{v_\perp^2 + v_\parallel^2} = \frac{2v_q}{\epsilon}\sqrt{1-\cos(\epsilon\tau)} \le \frac{2\sqrt{2}v_q}{\epsilon}. \tag{63}$$

Using the expression for $v_\perp$, we write the equation for the axial motion

$$\frac{d^2\xi}{d\tau^2} + \frac{2v_q^2}{v_{ph}^2\epsilon}[1-\cos(\epsilon\tau)]\xi = 0. \tag{64}$$

This equation can be cast in the standard form of the Mathieu equation (Ref. 37, p. 175)

$$\frac{d^2\xi}{dx^2} + [\tilde{a} - 2\theta\cos(2x)]\xi = 0, \tag{65}$$

where

$$\tilde{a} \equiv \frac{8v_q^2}{v_{ph}^2\epsilon^3}, \quad \theta \equiv \frac{\tilde{a}}{2}, \quad x \equiv \frac{\epsilon\tau}{2}. \tag{66}$$

Equation (64) describes an oscillator with a periodically changing frequency, such as a LC circuit with a periodically changing capacitance. The time-dependent oscillation frequency is

$$\omega_{osc}^2 = \omega^2\frac{2v_q^2}{v_{ph}^2\epsilon}[1-\cos(\epsilon\tau)], \tag{67}$$

and the maximal frequency is

$$\frac{\omega_{osc,\max}}{\omega} = \frac{2v_q}{v_{ph}\sqrt{\epsilon}} = 0.079. \tag{68}$$

The numerical value in Eq. (68) is obtained for our choice of parameter values as mentioned above. Equation (64) exhibits parametric oscillations when the difference between the cyclotron frequency and the wave frequency is close to the maximal oscillation frequency (67). Then ϵ is approximately $\epsilon_{\max}$ (57). This case will be addressed in a future study.

Figure 6 shows z and Fig. 7 shows v_z as functions of τ, as solutions of Eq. (29). The evolution is similar to that exhibited by the solution of the Mathieu equation [Eq. (64)] and by the approximate expression (62). The amplitude of the oscillations around the node first decreases, accompanied by an increasing oscillation frequency and increasing both perpendicular velocity and axial velocity (while crossing the node). At each of the necks in Fig. 6, $\omega_{osc}, v_\perp, v_\parallel$, and $v_z(z=\pi/4k)$ are maximal. After reaching a minimum, as time passes, the amplitude of the oscillations grows while the oscillation frequency decreases, following a decrease in all velocity components. When the oscillation frequency is zero $[\cos(\epsilon\tau)=1]$, the axial excursion is maximal, as expressed by the peaks in Fig. 6. There is a series of alternating maxima and minima of the oscillation amplitude and of the velocities with a time period,

$$\tau_p = \frac{2\pi}{\epsilon} = 2\pi\times 10^5. \tag{69}$$

The time period between successive maximal axial excursions is

$$\Delta\tau = \frac{\pi}{\epsilon} = 10^5\pi,$$

as is also seen in Fig. 6. Figures 8 and 9 show, respectively, the oscillations in time of $v_\perp$ and of $v_\parallel$, obtained as solutions of Eq. (29), which are in good agreement with (62).

We now examine the dynamics for

$$\tau \ll \frac{\pi}{2\epsilon} \Rightarrow \frac{d^2\xi}{d\tau^2} + \frac{v_q^2\epsilon}{v_{ph}^2}\tau^2\xi = 0. \tag{70}$$

As noted above, this is an equation for an oscillator of an increasing-in-time spring constant. It also describes a decreasing-in-time

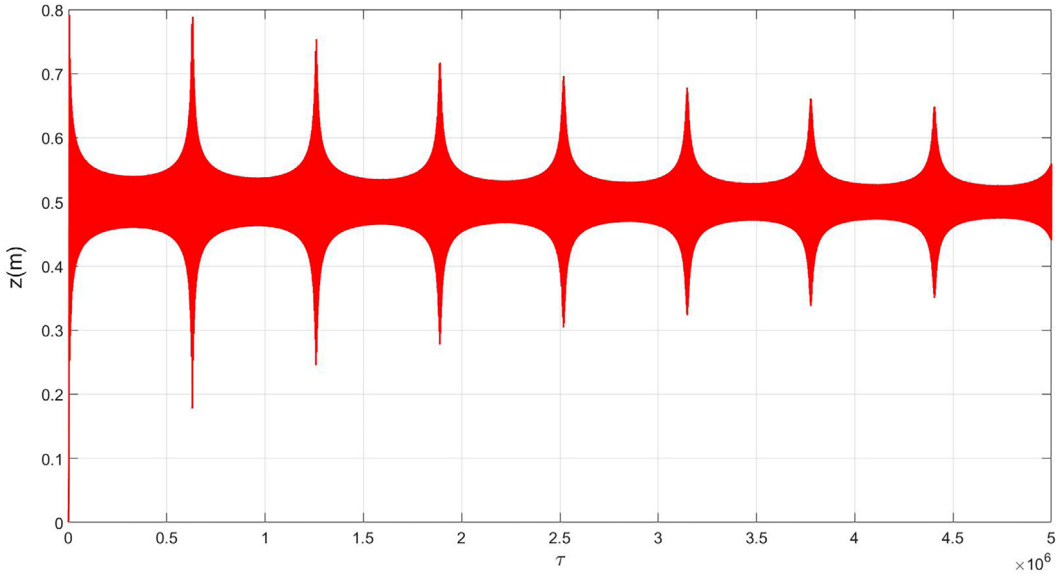

FIG. 6. $^6Li^+$ axial trajectory, z vs τ, under the fields of Fig. 1 for $\epsilon = 10^{-5}$.

01 April 2024 17:23:20

© Author(s) 2024

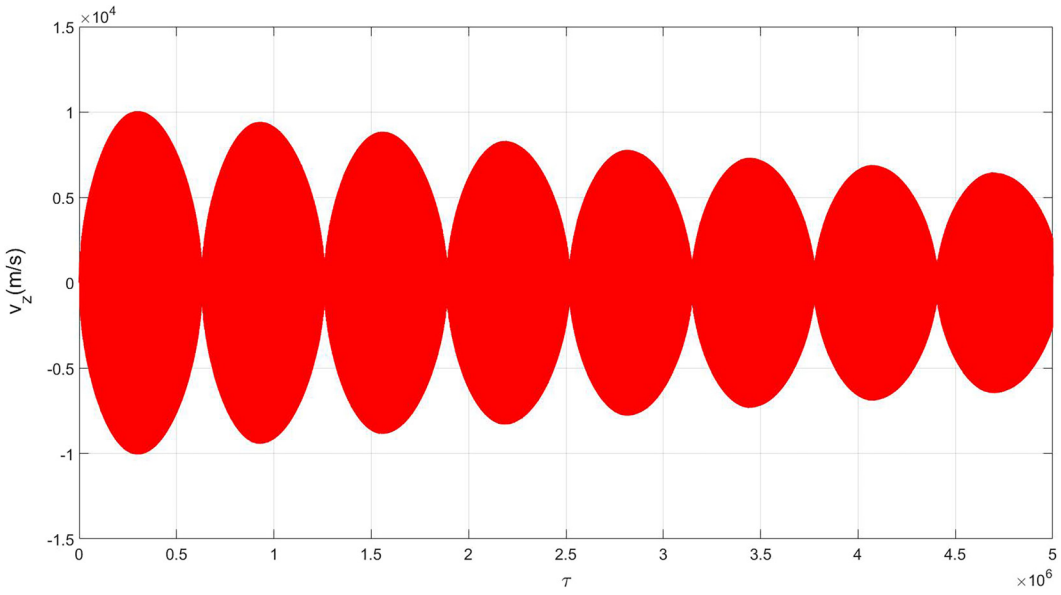

FIG. 7. $^6Li^+$ axial velocity, v_z vs τ, under the fields of Fig. 1 for $\epsilon = 10^{-5}$.

capacitance in an LC circuit, for example, by enlarging the distance between the capacitor plates by exerting a constant force. The equation is transformed into

$$\frac{d^2\xi}{ds^2} + \left(\frac{s^2}{4} - p\right)\xi = 0, \tag{71}$$

where

$$s = \left(\frac{2v_q}{v_{ph}}\right)^{1/2} \epsilon^{1/4}\left(\tau + \frac{v_{\|0}}{\sqrt{2}v_q}\right) \tag{72}$$

and

$$p \equiv \frac{1}{\sqrt{2\epsilon}}\frac{v_q}{v_{ph}}\left(\epsilon\frac{\sqrt{2}v_{\|0}^2}{4v_q^2} - \frac{v_{\perp 0}}{v_q}\right). \tag{73}$$

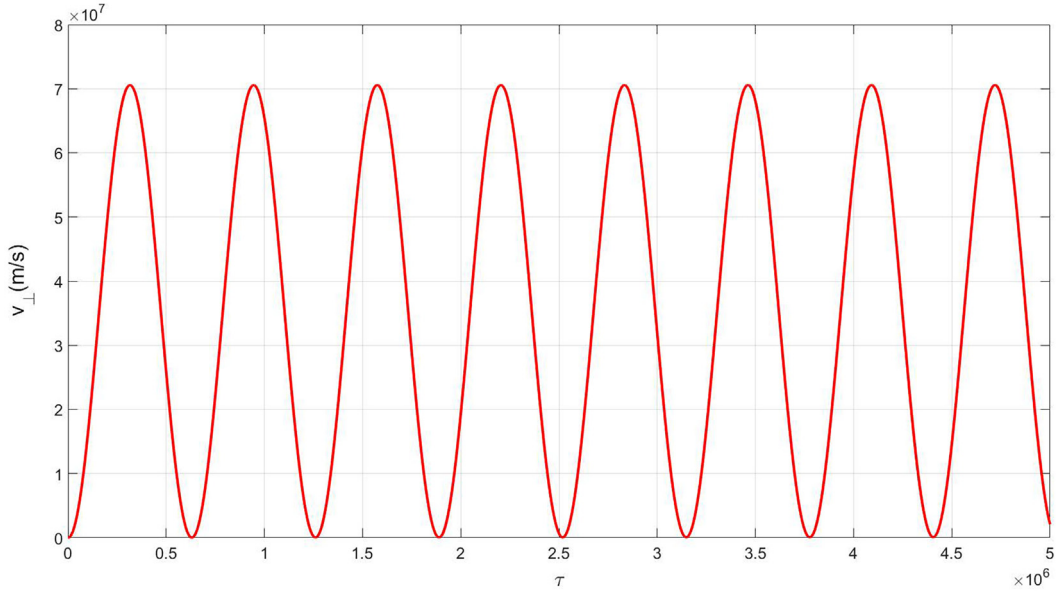

FIG. 8. $^6Li^+$ perpendicular velocity, $v_\perp$ vs τ, under the fields of Fig. 1 for $\epsilon = 10^{-5}$.

01 April 2024 17:23:20

© Author(s) 2024

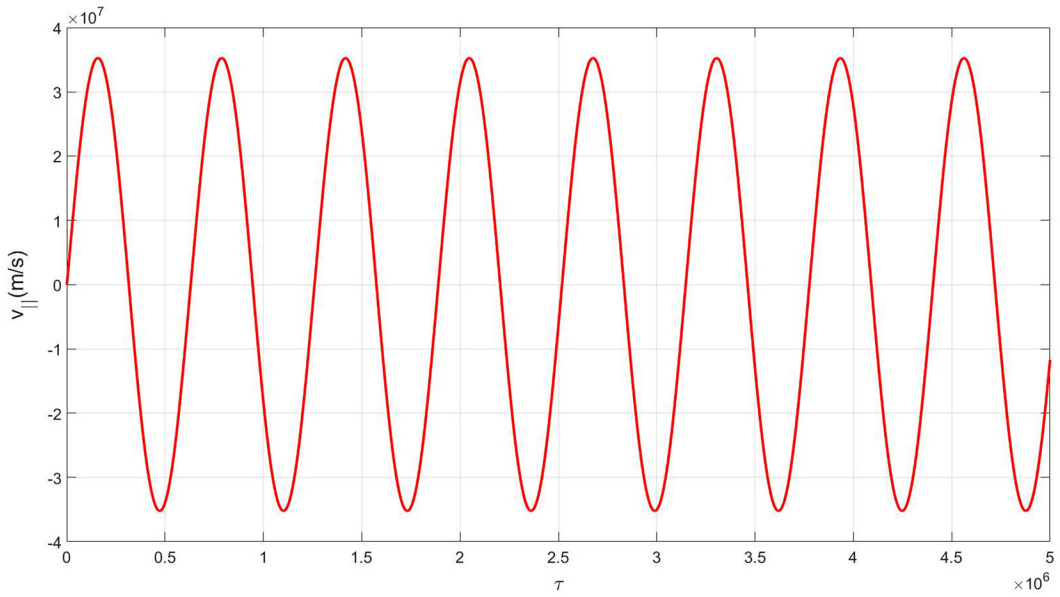

FIG. 9. $^6Li^+$ perpendicular velocity, $v_{\|}$ vs τ, under the fields of Fig. 1 for $\epsilon = 10^{-5}$.

Equation (71) is Weber's equation (Ref. 37, p. 159). Two independent solutions are[38]

$$\xi_1 = \exp\left(-\frac{is^2}{4}\right) M\left(-\frac{ip}{2}+\frac{1}{4};\frac{1}{2};\frac{is^2}{2}\right) \tag{74}$$

and

$$\xi_2 = s\exp\left(\frac{1}{4}i\pi\right)\exp\left(-\frac{is^2}{4}\right) M\left(-\frac{ip}{2}+\frac{3}{4};\frac{3}{2};\frac{is^2}{2}\right), \tag{75}$$

where $M(a,b,z)$ is the confluent hypergeometric function. We have constructed a solution that is a linear sum of the solutions (74) and (75),

$$\xi(s) = c_1\xi_1(s) + c_2\xi_2(s). \tag{76}$$

The coefficients c_1 and c_2 were determined by matching the expression (76) to the numerical solution of Eq. (29) (for $\epsilon = 10^{-5}$) at two neighboring values of s ($v_{\perp 0}$, and $v_{\|0}$ were taken as the values of the numerical solution at the smaller s of the two). The two s values, at which the matching was done, were at z values at which the linear approximation

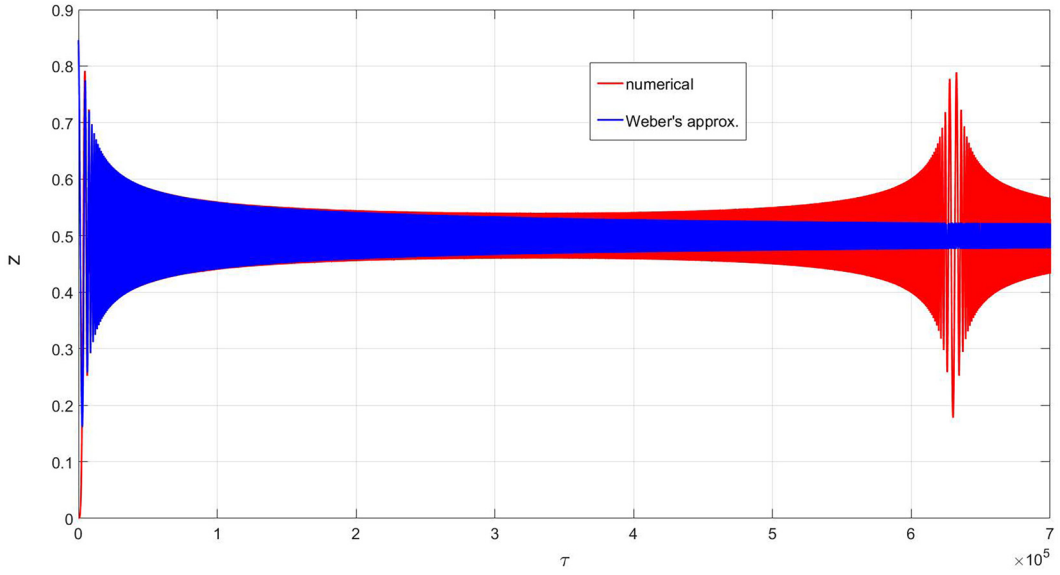

FIG. 10. $^6Li^+$ axial trajectory, z vs τ, under the fields of Fig. 1 for $\epsilon = 10^{-5}$. Comparison of the numerical solution (29) with the analytical solution (76) of Weber's equation (71).

01 April 2024 17:23:20

© Author(s) 2024

(59) held. Figure 10 shows z vs τ for both analytical solution (76) and numerical solution of Eq. (29). It is seen that for $\tau \ll \pi/2\epsilon$, the regime of validity of Weber's equation, the two solutions agree very well. The asymptotic expression for ξ [Eq. (76)] in this regime $\xi \sim \exp(is^2/4)$ expresses oscillations with a frequency increasing linearly in time, corresponding to $\omega_{osc}^2 \sim \tau^2$ in this regime [Eqs. (67) and (70)].

VI. SUMMARY

We have analyzed the ponderomotive force exerted by planar standing electromagnetic waves on ions that their cyclotron frequencies are close to the wave frequency. The direction of pushing along the magnetic field was shown to depend on the ion mass through the cyclotron frequency, allowing mass separation. We first used a simplified analytical single-particle analysis to clarify the mechanism of axial pushing. The analytic calculations were supported by numerical solutions of the equations of motion. It was shown that ions with a cyclotron frequency higher than the wave frequency are pushed to and oscillate around the wave magnetic node, while ions of a cyclotron frequency lower than the wave frequency are pushed toward and oscillate around the wave electric node. A detailed analysis was performed for the ion dynamics at the neighborhood of the wave magnetic node.

The ponderomotive force, being second order in the wave fields, is weak when an electromagnetic wave is used, since the wave magnetic field is weak. This makes the process weaker than other separation processes that use electromagnetic waves, such as ICR, which is first order in the wave fields. In the future, other configurations will be examined, in which the ponderomotive force is larger, so that the process is less vulnerable to collisions and plasma space-charge fields.

ACKNOWLEDGMENTS

This research has been partially supported by the Israel Science Foundation (Grant No. 2520/22).

AUTHOR DECLARATIONS

Conflict of Interest

The authors have no conflicts to disclose.

Author Contributions

A. Fruchtman: Conceptualization (lead); Formal analysis (lead); Writing – original draft (lead). **G. Makrinich:** Conceptualization (equal); Investigation (equal); Writing – review & editing (equal).

DATA AVAILABILITY

The data that support the findings of this study are available from the corresponding author upon reasonable request.

REFERENCES

[1]S. Z. Zweben, R. Gueroult, and N. J. Fisch, "Plasma mass separation," Phys. Plasmas **25**, 090901 (2018).
[2]A. J. Dempster, Phys. Rev. **11**, 316 (1918).
[3]W. E. Parkins, "The uranium bomb, the calutron, and the space-charge problem," Phys. Today **58**(5), 45 (2005).
[4]B. Lehnert, Nucl. Fusion **11**, 485 (1971).
[5]B. Bonnevier, "Plasma mass separation," Plasma Phys. **13**, 763 (1971).
[6]M. Krishnan, M. Geva, and J. L. Hirshfield, "Element and isotope separation in a vacuum arc centrifuge," Phys. Rev. Lett. **46**, 36 (1981).
[7]M. Geva, M. Krishnan, and J. L. Hirshfield, "Element and isotope separation in a vacuum-arc centrifuge," J. Appl. Phys. **46**, 1398 (1984).
[8]T. Ohkawa and R. I. Miller, "Band gap ion mass filter," Phys. Plasmas **9**, 5116 (2002).
[9]J. Gilleland, S. Agnew, B. Cluggish, R. Freeman, R. Miller, S. Putvinski, L. Sevier, and K. Umstadter, "Application of archimedes filter for reduction of Hanford HLW (high level waste)," in *WM Symposia*, 24–28 February 2002, Tucson, AZ, 2002.
[10]R. Freeman, S. Agnew, F. Anderegg, B. Cluggish, J. Gilleland, R. Isler, A. Litvak, R. Miller, R. O'Neill, T. Ohkawa, S. Pronko, S. Putvinski, L. Sevier, A. Sibley, K. Umstadter, T. Wade, and D. Winslow, AIP Conf. Proc. **694**, 403 (2003).
[11]S. Shinohara and S. Horii, "Initial trial of plasma mass separation by crossed electric and magnetic fields," Jpn. J. Appl. Phys. Part 1 **46**, 4276 (2007).
[12]V. P. Smirnov, A. A. Samokhin, N. A. Vorona, and A. V. Gavrikov, "Study of charged particle motion in fields of different configurations for developing the concept of plasma separation of spent nuclear fuel," Plasma Phys. Rep. **39**, 456 (2013).
[13]G. Liziakin, N. Antonov, V. S. Smirnov, R. Timirkhanov, A. Oiler, R. Usmanov1, A. Melnikov, N. Vorona, S. Kislenko, A. Gavrikov, and V. P. Smirnov, "Plasma mass separation in configuration with potential well," J. Phys. D **54**, 414005 (2021).
[14]A. J. Fetterman and N. J. Fisch, "The magnetic centrifugal mass filter," Phys. Plasmas **18**, 094503 (2011).
[15]R. Gueroult, E. S. Evans, S. J. Zweben, N. J. Fisch, and F. Levinton, "Initial experimental test of a helicon plasma based mass filter," Plasma Sources Sci. Technol. **25**, 035024 (2016).
[16]R. Gueroult, J.-M. Rax, and N. J. Fisch, Phys. Plasmas **21**, 020701 (2014).
[17]R. Gueroult and N. J. Fisch, "Plasma mass filtering for separation of actinides from lanthanides," Plasma Sources Sci. Technol. **23**, 035002 (2014).
[18]I. Ochs, R. Gueroult, N. J. Fisch, and S. J. Zweben, "Collisional considerations in axial-collection plasma mass filters," Phys. Plasmas **24**, 043503 (2017).
[19]I. S. Averbukh, M. J. J. Vrakking, D. M. Villeneuve, and A. Stolow, Phys. Rev. Lett. **77**, 3518 (1996).
[20]J. M. Dawson, H. C. Kim, D. Arnush, B. D. Fried, R. W. Gould, L. O. Heflinger, C. F. Kennel, T. E. Romesser, R. L. Stenzel, A. Y. Wong, and R. F. Wuerker, "Isotope separation in plasmas by use of ion cyclotron resonance," Phys. Rev. Lett. **37**, 1547 (1976).
[21]A. C. La Fontaine, d P. Louvet, P. L. Le Gourrierec, and A. Pailloux, J. Phys. D **31**, 847 (1998).
[22]V. I. Volosov, I. A. Kotelnikov, and S. G. Kuzmin, "Separation of heavy-element isotopes by selective ICR heating techniques," Plasma Phys. Rep. **24**(6), 474–485 (1998) [translated from Fiz. Plazmy **24**(6), 517–529 (1998)].
[23]J. M. Rax, J. Robiche, and N. J. Fisch, Phys. Plasma **14**, 043102 (2007).
[24]A. V. Timofeev, "Plasma method for processing spent nuclear fuel," Plasma Phys. Rep. **33**, 890 (2007); Fiz. Plazmy **33**, 971 (2007).
[25]D. A. Dolgolenko and Y. A. Muromkin, "Plasma isotope separation based on ion cyclotron resonance," Phys.-Usp. **52**(4), 345–357 (2009).
[26]A. V. Timofeev, "On the theory of plasma processing of spent nuclear fuel," Phys.-Usp. **57**(10), 990 (2014).
[27]D. A. Dolgolenko and Y. A. Muromkin, "Separation of mixtures of chemical elements in plasma," Phys.-Usp. **60**(10), 994–1017 (2017).
[28]D. A. Dolgolenko, Y. A. Muromkin, and V. G. Pashkovskya, Instrum. Exp. Tech. **62**, 798–808 (2019).
[29]E. S. Weibel, "Separation of isotopes," Phys. Rev. Lett. **44**, 377 (1980).
[30]M. S. Festeau-Barrioz and E. S. Weibel, "Ponderomotive force of an ion cyclotron wave in a two-ion species plasma," Phys. Fluids **23**, 2045 (1980).
[31]E. S. Weibel and M. S. Festeau-Barrioz, "Ponderomotive effect in a two ion species magnetized and bounded plasma," Plasma Phys. **24**, 256 (1982).
[32]T. Ohkawa, "Plasma mass separator using ponderomotive forces," US patent 6,585,891B1 (2003).
[33]H. Motz and C. J. H. Watson, Adv. Electron. Electron Phys. **23**, 153 (1967).
[34]T. H. Stix and R. W. Palladino, "Experiments on ion cyclotron resonance," Phys. Fluids **1**, 446 (1958).
[35]A. Fruchtman and H. Weitzner, "Fundamental ion-cyclotron frequency heating in tokamaks," Phys. Fluids **29**, 1620 (1986).
[36]D. Van Eester, E. Lerche, R. Ragona, A. Messiaen, T. Wauters, and JET Contributors, "Ion cyclotron resonance heating scenarios for DEMO," Nucl. Fusion **59**, 106051 (2019).
[37]E. L. Ince, *Ordinary Differential Equations* (Dover, New York, 1956).
[38]*Handbook of Mathematical Functions With Formulas, Graphs, and Mathematical Tables*, *Applied Mathematics Series* Vol. 55, edited by M. Abramowitz and I. Stegun (Dover Publications, 1972).

01 April 2024 17:23:20

© Author(s) 2024